

# Novel method for quantitative starch penetration analysis through iodine staining and image analysis of cross-sections of uncoated fine paper

Juha Lipponen, Metso Paper, Inc., Finland, Timo Lappalainen, VTT Processes, Finland, Jouni Astola, Raisio Chemicals, Finland and Johan Grön, StoraEnso, Finland

**KEYWORDS:** Cross-section, Iodine staining, Image analysis, Starch, Penetration

**SUMMARY:** This paper presents a novel method for determining starch penetration through iodine staining and microscopic imaging of surface-sized fine paper cross-sections and image analysis of the resulting grayscale images. The more specific aim was to obtain quantitative starch penetration information in the z-direction of the sheet. The penetration information was determined through an image analysis procedure as a z-directional distribution of pixels classified to contain starch based on their grayscale values. This analysis was conducted on a number of cross-sectional images to improve the accuracy of the analysis since the variation of starch penetration within the scope of a single cross-sectional image varies across a large window. The numerical penetration information obtained was used in further processing, such as determining a dimensionless penetration number  $Q$ . The penetration number can be quantitatively used in comparing the penetration of starch in different paper samples produced under different process conditions, for example, that affect surface size starch penetration. Therefore, the penetration number  $Q$  can be used in characterizing penetration-related paper properties – such as the internal strength of the sheet – to help in the optimization of starch penetration-related papermaking process parameters. The penetration information was also processed to represent a starch amount distribution in the z-direction, defined here as a Simulated Starch Content (SSC) distribution. This SSC distribution gives a good estimate of the starch distribution across the z-direction. The method developed in this work is fast and it will give quantitative and comparable information on z-directional starch penetration. Since the complete procedure was defined in detail from the handling and iodine staining of the specimens to the microscopic photographing of the cross-sections and computational image analysis of the cross-sectional images, the results are not dependent on individual personal factors of the personnel conducting the analysis. The starch penetration curves were also compared against Li-distributions obtained through ToF-SIMS, that represented the distribution of the starch solution in the z-direction, using  $\text{LiCl}_2$  as a marker for starch.

**ADDRESSES OF THE AUTHORS:** Juha Lipponen (juha.lipponen@metso.com): Metso Paper, Inc., Process Technology, Wärtsilänkatu 100, 04400 Järvenpää, Finland.  
Timo Lappalainen (timo.lappalainen@vtt.fi): VTT Processes, P.O. Box 1603, 40101 Jyväskylä.  
Jouni Astola (jouni.astola@raisio.com): Raisio Chemicals Oy, PO Box 101, 21201 Raisio and Johan Grön (johan.gron@storaenso.com): StoraEnso Publication Paper, Book and News Business Unit, 46900 Finland.

Starch penetration and the consequent z-distribution of starch in the sheet are often discussed when different sur-

face sizing methods or process variables, such as solids contents or viscosity levels, are evaluated against the properties of paper (e.g. Hoyland et al. 1977; Wight 1988; Sollinger 1988; Küstermann 1990; Ryder 1997). These conclusions are often supported by qualitative evaluations of cross-sectional images describing the starch penetration (e.g. Fineman and Hoc 1978; Bergh 1984; Hansson and Klass 1984; Rantanen and Westergård 1987; Bergh and Åkesson 1988; Tehomaa et al. 1992; Kimpimäki and Rennes 2000; Lipponen et al. 2002). Here, paper properties are assumed to reflect the penetration behavior of starch. Cross-sectional images are then used to support the conclusions made based on differences in starch penetration. Cross-sectional images with iodine staining are prepared by dipping paper samples in a solution of iodine potassium iodide (I-KI), whereby the starch in the sheet structure is dyed dark. An image is then acquired from the cross-section with a light microscope. This method is fast and inexpensive compared to the microtome preparation procedure, for example. However, the process stages of the iodine staining penetration evaluation method are not standardized and the cross-section images are analyzed only visually. Further, a single cross-section – usually cut less than a millimeter in length – leaves the observation vulnerable to local variations in starch penetration caused by the properties of the base sheet, such as flocculation. This would then introduce a great deal of uncertainty into this type of evaluation of starch penetration. Iodine staining is also a well-known method for the determination of starch on the paper surface. Zsoldos and Sebess (1975) present a new method for the determination of starch on the paper surface. In their method, the starch iodine reaction is performed in two stages: the water amount required for the reaction is achieved through water vapor condensation on the paper surface, and the required amount of iodine is sublimated from solid crystalline iodine.

Microtomic cross-sections are often used in illustrating paper structure in the z-direction. Preparing the microtomic cross-sections requires embedding the specimen in epoxy resin and curing it for a considerable period of time. The resulting blocks are then ground and polished. The final cross-sections are thereafter cut to thin slides for light microscope viewing, or further prepared for SEM analysis (e.g. Peterson and Williams 1992). Bailey and Bown (1990) use cross-sectional images for the qualitative evaluation of filler and coating color distributions in the paper sheet. SEM images are also used as a basis for the z-directional structural characterization of

paper through image analysis of the cross-sections (Allem 1998, Grön and Ahlroos 1998, Allem and Uesaka 1999, Dickson 2000, Chinga and Helle 2002). However, in the examination of highly variable structures such as paper, small scale samples obtained with microtomic sectioning fail to fully represent significant structural features of the sheet. Williams and Drummond (1994) described an improved method for preparing large microtomic cross-sections for SEM analysis, presenting a polishing method conventionally used for the preparation of polished metallographic sections. With the method presented, samples of 200 mm total width could be prepared in less than 2 hours. However, the curing of resin still requires up to two days. In examining the cross-sections obtained through SEM, for example, grayscale segmentation based on thresholding grayscale histograms of digital images is a common approach. Manual thresholding, however, will vary between operators and even with one person over time. To avoid any subjective dependence in the thresholding of grayscale images on personal factors (Tovey and Hounslow 1995; Barratte et al. 1997), automated procedures are important to improve repeatability and to reduce subjectivity, as well as arduous work.

The ToF-SIMS (Time of Flight Secondary Ion Mass Spectroscopy) technique is used to analyze solid samples. This technique combines high surface sensitivity with low detection limits and high mass resolution. With the ToF-SIMS technique, it is possible to make distribution maps of ions with good spatial resolution. This technique is used, for instance, in probing the chemistry of surfaces (Kulick and Brinen 1998), in detecting desizing agents (Brinen and Kulick 1995), in analyzing AKD (Zimmermann and Hercules 1995), in detecting trace elements in wood (Bailey and Reeve 1994), and in analyzing printed papers (Preston et al. 2000).

If a quantitative starch distribution analysis method providing reliable and repeatable information on starch penetration were available, more fundamental knowledge could be obtained of parameters affecting the penetration of starch. Surface sizing and base paper parameters and their effect on starch penetration – and on the desired paper properties obtained through starch – could then be investigated in much greater detail. Therefore, the aim of this study was to further develop the iodine staining starch penetration evaluation method. Here, one of the critical factors in the study was to set up a standardized procedure for preparing and photographing the iodine stained cross-sections. This way image acquisition would not be dependent on personal factors. A further objective was to establish automated image analysis of the cross-sectional images obtained. The final aim was to develop a method for producing quantitative and comparable starch penetration curves and also a parameter for characterizing the z-directional penetration of starch, i.e. a dimensionless penetration number. This parameter could then be used in interpreting starch penetration-related paper properties. This information could, in turn, be used in evaluating and optimizing the papermaking parameters that influence starch penetration in the surface sizing process.

## Materials and Methods

### Sample preparation

A modified potato-based starch (Raisamyl 01020, Raisio Chemicals Inc., Raisio, Finland) was used in producing the surface sized samples in our study. A native potato starch was initially modified through oxidation with hypochlorite, and the carboxylic group content in the oxidized starch was about 1% ( $DS_{-COOH} = 0.031$ ). The viscosity of the starch was 20 mPas (Brookfield 100 rpm, 60 °C) at a concentration of 10%. 1 g of  $LiCl_2$  per 1000 g dry starch was added as a starch indicator under the ToF-SIMS method used for comparison in our study. A wood-free base paper without surface sizing and a basis weight of 82  $g/m^2$  was used for the study. The properties of the base paper are presented in *Table 1*.

Table 1. Properties of Base Paper.

Properties		Values
Grammage	$g/m^2$	82
Ash content	%	14.7
Internal sizing	%	0.8
Air permeability, Bendtsen	ml/min	775
Internal strength, Scott Bond	$J/m^2$	147

The trials were run as a C2S MSP application (OptiSizer, Metso Paper, Inc.) at a speed of 1200 m/min and a linear load of 25 kN/m. The roll cover material was polyurethane, with a hardness of 36 P&J and roll diameter of 950 mm. Film metering was performed with both 10 mm grooved rods and 15 to 35 mm smooth rods to obtain a constant dry starch amount of approximately 1  $g/m^2$ /side with different starch solids contents. The solids content levels used were 8%, 12%, 15% and 18%, with starch amounts of 1.8, 2.0, 2.0 and 1.8  $g/m^2$ , respectively. A single nip soft calender was used at a machine speed of 1200 m/min, a steel roll temperature of 60 °C, and a linear load of 45 kN/m. The topside of the paper was run against the steel roll. The hardness of the polymer roll was 90 ShD and diameter 420 mm.

The internal strength of the sheet was measured according to TAPPI T833 om-96. The total starch amount applied was measured from the paper samples using lithium chloride analysis (Mendham et al. 2000), where a weighed portion of the sample is burned in a muffle furnace. The residue is dissolved in acid and the individual element concentration is then determined with ICP-AES (Inductively Coupled Plasma Atomic Emission Spectroscopy).

The paper samples were cut in the machine direction with a surgical blade fastened to the side of a smooth based metal block. Cutting was performed on a hard plastic plate. The surface of the cross-section was thus as smooth and planar as possible to give a clear and focused image of the whole cross-section under the microscope. A smooth surface was also necessary for uniform absorption of the I-KI solution into the cross-sectional surface. The blade was replaced after cutting 50 strips. The cross-sectional surface of the strip was then dipped in a 1–2 ml dose of 0.1 M iodine potassium iodine (I-KI)

solution, which was pipetted into a separate glass bowl from a light-protected vessel immediately before the dipping. The I-KI solution was replaced after each dipping to ensure its purity and to keep light from weakening the dyeing reaction. The strip moistening time was approximately 1 s. After the dipping, excess I-KI solution was removed from the specimen by pressing a blotting board on the top and bottom surfaces of the strip without touching the cross-sectional surface itself. The strip was then set under a microscope for photographing the iodine-stained cross-sectional surface. The cross-section of the moistened sample was photographed under a microscope using a Nikon Eclipse ME600 light microscope (Nikon Corporation, Kawasaki, Japan), a PCO 12-bit CCD camera (PCO Computer Optics GmbH, Kelheim, Germany) and a variable Fostec DCR II planar light source (Schott Fostec, Auburn, NY, USA). The field of view under the microscope was 0.85 x 0.68 mm, and the size of the RGB-image acquired of the cross-section was 1280 x 1024 pixels. The resolution of the image produced was therefore 0.664 mm/pixel. DF (Dark Field) illumination from above was used to light the specimen under the microscope. After manually focusing the image, specimens creating deep shadows (i.e. the edges of the cross-section not clearly visible) due to excessive cockling of the strip were discarded at this stage. Here, shadows at the edges of the cross-sectional image could distort the following grayscale image analysis.

When changing the parameters of the cross-sectional imaging, e.g. a change in the exposure time  $t_{exp}$ , a reference target – a plastic slip of standardized lightness – was required for the determination of changes in the quantity of lightreaching the CCD sensor, i.e. for the calibration of the imaging parameters to ensure the comparability of the images. The lightness of the reference target is  $L = 34$ , determined by spectrophotometry. The value of the global threshold,  $T_{exp}$ , used in the segmentation of the image was determined as follows:

$$T_{t_{exp}} = \langle GR \rangle_{t_{exp}} + T_{Bias} \quad [1]$$

where  $\langle GR \rangle_{t_{exp}}$  was the mean of the grayscale histogram in an image of the reference target with exposure time  $t_{exp}$ , and  $T_{Bias}$  was the global threshold, which was used to select the darkness of pixels classified as starch. The grayscale threshold determined for the reference target using the illumination time  $t_{exp}$  was always employed for segmenting cross-section images acquired using the same exposure time.

### Image analysis of the cross-sectional images and acquisition of penetration curves

At the first stage of the image analysis, the location of the cross-section in the original 1280 x 1024 image was roughly determined using the contrast between the background and the strip itself. This was performed by segmenting the grayscale image into a two-level (binary) image  $\mathbf{B}(i,j)$  of the grayscale cross-section. Thus, pixels labeled 1 correspond to the strip and pixels labeled 0 correspond to the background. When a projection was

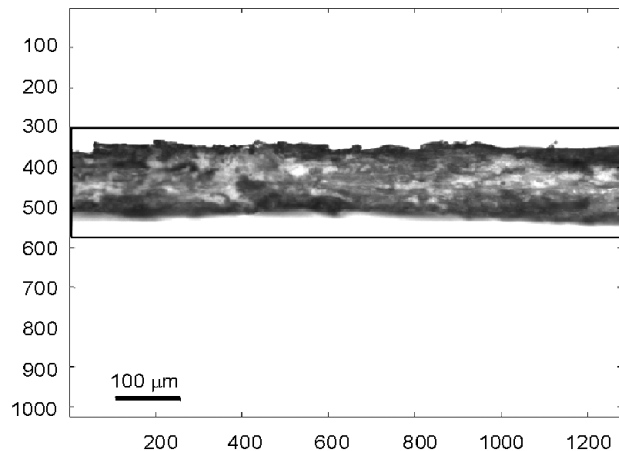


Fig 1. Identification of the position of the cross-section on the area of the original microscopical digital image. The Region Of Interest (ROI) – where the following image analysis is performed – is presented as a rectangle around the cross section.

calculated from the binary image on the y axis, the first estimate for the location of the strip in the image was obtained. A rectangle within the sample to be analyzed was then chosen as the Region Of Interest, ROI (Fig 1). At the subsequent stages of image processing only this ROI was analyzed. This way the following image analysis required less computing power than analyzing the whole original 1280 x 1024 image.

Then, the binary image  $\mathbf{B}(i,j)$  was analyzed column by column in order to identify the edges (i.e. the top and bottom surface curves) of the cross-sectional image. If there were bright undyed areas in the cross-sectional image, it was possible that the edges of the cross-sectional image could not be able to be identified correctly in some columns of the matrix  $\mathbf{B}(i,j)$ . Therefore, the vectors of edge points  $z_{top}$  and  $z_{bottom}$  were filtered with a median filter. Vectors containing values of edge pixels  $z_{top}$  or  $z_{bottom}$  can be presented as follows:

$$\begin{aligned} z &= z_{top} \quad \text{or} \quad z = z_{bottom} \\ G1(x_i) &= \text{med}(z(x_{i-L1}), \dots, z(x_i), \dots, z(x_{i+L1})) \\ G2(x_i) &= \text{med}(z(x_{i-L2}), \dots, z(x_i), \dots, z(x_{i+L2})) \\ G_{top}(x_i) &= \max(G1(x_i), G2(x_i)) \\ G_{bottom}(x_i) &= \min(G1(x_i), G2(x_i)) \end{aligned} \quad [2]$$

where  $G1(x_i)$  and  $G2(x_i)$  are median filtered vectors,  $L1 > n * L2$ ,  $n \geq 5$  and  $G_{top}(x_i)$  and  $G_{bottom}(x_i)$  are the filtered vectors containing values of edge pixels in the top and bottom edge of the cross-sectional image. As seen in Fig 2, the filtration of vectors effects more the outward objects than the inward ones. Fibers and fines pointing outward from the surface (i.e. fibers torn off from the surface during the cutting of the cross-sectional surface) could thus be filtered from the cross-sectional image. The determined edge does, however, follow the surface to the bottom of any pores.

At the next stage of image processing, only the area between the detected top and bottom edges of the cross-sectional image was analyzed. Here, the area between the detected edges of the cross-section in the grayscale image was segmented using the global threshold  $T_{t_{exp}}$  (Eq 1).  $T_{t_{exp}}$  was the standard grayscale threshold, which was

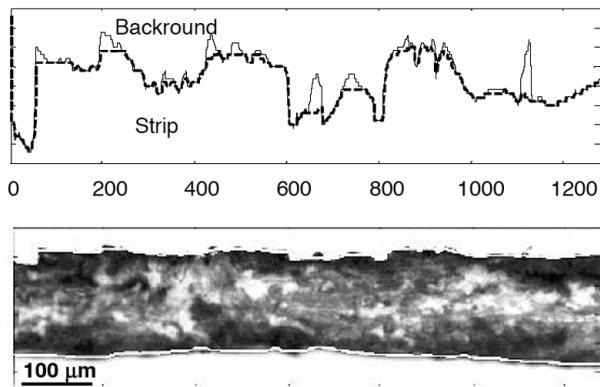


Fig 2. The edge detection method is illustrated using the top edge of the strip (top). The vector containing the values of edge pixels  $Z_{top}(x_i)$  is presented as a solid line and the median filtered one  $G_{top}(x_i)$  as a dashed line (i.e. the determined top side edge curve of the strip). The bottom figure illustrates the completed top and bottom edge detection fitted on an image of the cross-section.

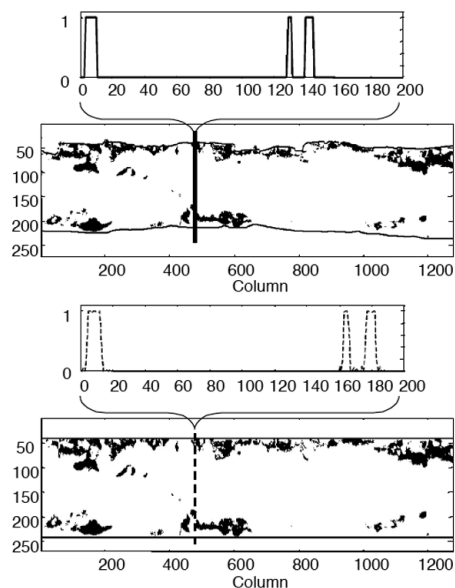


Fig 3. Original binary image with an illustration of a single sequence (top), and a thickness-normalized binary image with an illustration of a resampled sequence (bottom). The equalized thickness,  $w$ , of the resampled sequence is 200 normalized units.

used to determine how dark pixels were classified as starch. In our study, the threshold value  $T_{Bias}$  was determined by making a similar cross-sectional image of a base paper sample not containing surface sizing starch.  $T_{Bias}$  was set to a level at which less than 0.8% of the pixels in the base paper – based on the wet end starch content of the paper – were under the global threshold  $T_{exp}$ . The purpose of this approach was to calibrate the analysis of the dyeing reaction according to the wet end starch in the specimens. In our study, the threshold grayscale value  $T_{Bias}$  selected based on this condition was set at 16.

In order to determine the z-directional distribution of starch-containing pixels, cross-section thickness variations had to be removed during image analysis. Here, the thickness of the whole cross-section (i.e. all 1280 columns) was equalized by normalizing the length of the individual columns to a constant length of  $w = 200$  pixels. This procedure is illustrated in Fig 3. A cross-sectional image with binary starch location information

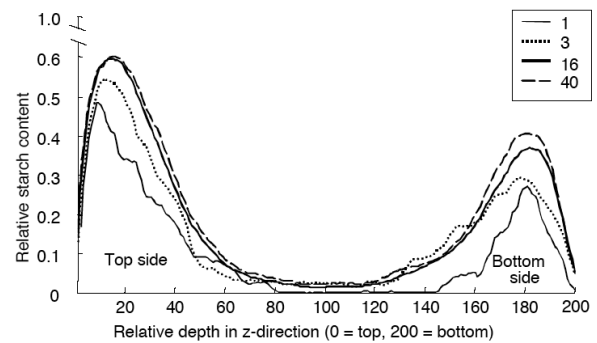


Fig 4. Starch penetration curves averaged from 1, 3, 16 and 40 cross-sectional images. These curves are obtained by averaging the corresponding number of cross-sections, each consisting of 1280 sequences. The relative starch content (between 0 and 1) in the y-axis describes the occurrence of pixels categorized to contain starch in the z-directional depth of the sheet.

within a cross-section of constant thickness was then available for acquiring a z-directional distribution curve of pixels classified to contain I-KI-stained starch in the original cross-sectional image.

As mentioned, the machine direction length of a single cross-section was only 0.85 mm. On the other hand, several process parameters and paper structure variations – such as flocculation – may affect starch penetration behavior on the order of several millimeters. Therefore, in order to gain reliable information of overall starch penetration and its effect on paper properties on the macro scale, starch penetration information needs to be averaged from a larger amount of data. Examples of starch penetration curves averaged from 1, 3, 16 and 40 cross-sectional images of 1280 normalized columns are shown in Fig 4. Increasing the number of measurements  $n$  will give a more reliable estimate of the distribution than any of the measurements taken alone. The standard deviation of the mean,  $s_x/\sqrt{n}$ , decreases slowly as  $n$  increases. It can be observed that the shape of the starch penetration curve obtained does not change significantly when 16 or more individual starch distributions are averaged. Then, 16 cross-sectional images were averaged to obtain the penetration curve for each specimen. Therefore, a total cross-sectional sample length of 13.6 mm in the machine direction was included in the determination of the starch penetration analysis.

#### Definition of a Dimensionless Penetration Number, $Q$ and the Simulated Starch Content Distribution, $SSC(Z)$

Once a usable method for determining a quantitative penetration curve is available, one might suggest that it would also be useful to describe a single dimensionless number to represent the relative penetration depth of starch. Such a number could then be used for the quantitative comparison of paper samples with different starch penetration levels. Further, a penetration number can be quantitatively used in comparing the penetration of starch in different paper samples (e.g. produced under different process conditions) to determine the function of any paper making variable whose contribution to surface sizing starch penetration behavior is of interest. Here, the thickness of paper was divided into four layers equal in

thickness, and the integrals (areas covered by the penetration curve) of these sections were defined as  $A_{0-50}$ ,  $A_{50-100}$ ,  $A_{100-150}$  and  $A_{150-200}$ . Now, the suggested penetration numbers  $Q_{top}$  and  $Q_{bottom}$  were defined at both the top and bottom sides separately as the ratio of the area covered by the penetration curve at the inner quarter of the sheet's thickness and the area covered by the penetration curve at the half thickness of the specimen. The mean penetration number  $Q_{tot}$  was then calculated as the weighed average of the penetration numbers obtained from the two sides as  $Q_{tot}$ . This definition of the penetration number  $Q$  is illustrated in Fig 5 and in Eq 3.

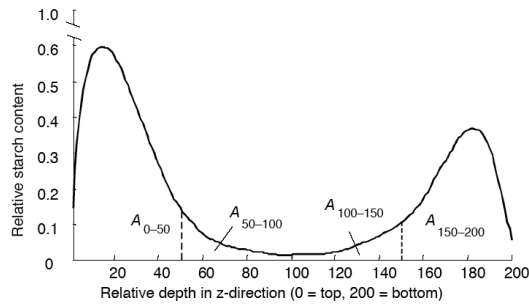


Fig 5. An illustration of the sectional areas  $A_{0-50}$ ,  $A_{50-100}$ ,  $A_{100-150}$  and  $A_{150-200}$  covered by the starch penetration curve obtained. These sectional areas are then used in the determination of the penetration number  $Q$ . The relative starch content (between 0 and 1) in the y-axis describes the occurrence of pixels categorized to contain starch in the  $z$  directional depth of the sheet.

$$\begin{aligned}
 Q_{top} &= \frac{A_{50-100}}{A_{0-50} + A_{50-100}} \\
 Q_{bottom} &= \frac{A_{100-150}}{A_{100-150} + A_{150-200}} \\
 Q_{tot} &= \frac{Q_{top}(A_{0-50} + A_{50-100}) + Q_{bottom}(A_{100-150} + A_{150-200})}{A_{0-50} + A_{50-100} + A_{100-150} + A_{150-200}}
 \end{aligned}
 \quad [3]$$

The characteristics  $Q_{top}$ ,  $Q_{bottom}$  and  $Q_{tot}$  are standardized within  $[0,1]$ . If starch is distributed evenly in the  $z$  direction, the value of  $Q_{tot}$  is 0.5. If  $Q_{tot} > 0.5$ , there is more starch in the inner parts of the cross-section sample than on its surfaces.

Starch penetration curves obtained with the method described here can, in principal, not be directly interpreted as starch content distributions, similarly to filler distribution analysis, since pixels of the cross-sections were only evaluated "to contain" or "not to contain" starch based on the threshold analysis described above without any scalar amount information of starch at individual pixels. However, when penetration curves with different specimens are compared, penetration curves processed to represent starch amount distributions in the  $z$ -direction using the separately measured starch amount can be of interest. Here, the quantitative starch penetration curves were used to illustrate the assumed starch content distribution by normalizing the integrals of the individual starch penetration curves (i.e. the covered area of the penetration curve) to correspond to the actual starch content in the specimens. If we define the starch penetration curve  $P$  as a function of thickness  $z$  as  $P(z)$ , the separately measured starch amount as  $\rho_{starch}$ , and the starch amount normalized Simulated Starch Content (i.e.

$SSC$ ) as a function of thickness as  $SSC(z)$ , and the equalized thickness as  $w$ , we can define

$$SSC(z) = \frac{\rho_{starch}}{w} \frac{\int P(z)}{P(z)} \quad [4]$$

Now we can plot the starch penetration curve as a simulated starch content curve  $SSC(z)$  giving an assumption of the starch amount distribution across the sheet thickness using units of weight per unit area (e.g.  $g/m^2$ ).

### Preparation of Samples for ToF-SIMS Analysis and Image Analysis of ToF-SIMS images

In our study, the ToF-SIMS method was employed as the method of comparison for the I-KI dyeing method of cross-sections. ToF-SIMS was used to identify the lithium ions of  $LiCl_2$  added to starch during the surface sizing process. Here,  $LiCl_2$  dissolved in the starch solution was expected to penetrate to the paper structure along with the starch. The distribution and amount of the  $LiCl_2$  was then meant to be traced from the cross-sectional images prepared.

Paper samples were embedded in epoxy resin and cross-sectioned. ToF-SIMS analyses were used to obtain ion distribution maps for the lithium ion in the cross-sections. The instrument used for the ToF-SIMS analysis was a PHI TRIFT II (ULVAC-PHI, Chigasaki, Japan). ToF-SIMS images were acquired in the positive ion mode at 25 kV accelerating voltages using a Ga liquid ion metal gun over a mass range of 2–2000 amu. The analyzed area was  $200 \times 200$  mm. Specimens (ca.  $2 \times 10$  mm) were cut in the machine direction. After cutting, the specimens were put in a flat embedding mold made of silicone rubber (Agar G369). The specimens were embedded in transparent cold mounting epoxy resin (Struers Epofix kit). An Epofix kit has two components, Epofix resin and Epofix hardener, which were mixed immediately before use (25 parts of resin and 3 parts of hardener by weight). Then the epoxy resin was allowed to cure at room temperature for about 8 hours. After the curing of the epoxy resin, the specimens were cross-sectioned in the machine direction with a Leica RM 2165 microtome (Leica Microsystems, Wetzlar, Germany). Cross-sections were made using a glass knife in order to obtain a smooth surface. The ToF-SIMS analysis of paper was made directly from the resulting epoxy block. Fig 6 represents an example of an overall ion image of the cross-section as well as the corresponding  $Li^-$  image of a paper sample with a starch solids content of 18% and a total starch amount of  $1.8 g/m^2$ .

The  $Li^-$  cross-sectional images were analyzed column by column similarly to the cross-sections treated with the I-KI dyeing method in order to determine the distribution of the  $Li$  ions across the  $z$ -direction. Edge detection begun with detecting the furthest top and bottom  $Li^-$  pixels from each column of the  $Li^-$  image (Fig 7, top). This group of pixels was classified in all columns  $i$  as edge pixels only when the distance  $w$  between the topmost and the lowest  $Li^-$  pixels in column  $i$  was  $w(I) > W_{min}$  pixels, the value of  $W_{min}$  being based on the thickness of the strip. In our study, the requirement for the minimum

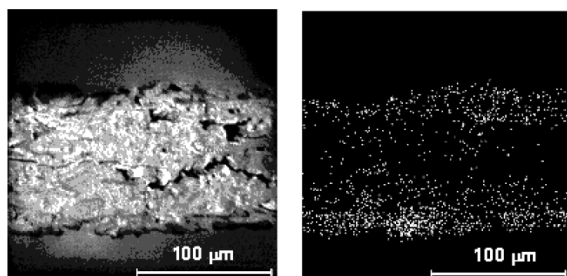


Fig 6. The total ion image of the cross-section (left) and the corresponding  $\text{Li}^-$  image (right). Bright dots in the image on the right indicate lithium ions.

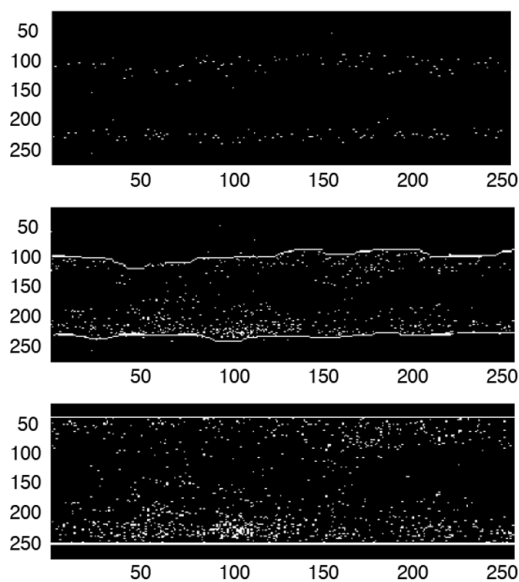


Fig 7. The furthest  $\text{Li}^-$  pixels at the low end and top end of each column of a  $\text{Li}^-$  image of the cross-section (top), median-filtered edge detection of the  $\text{Li}^-$  image, (middle), and the thickness-normalized  $\text{Li}^-$  image (bottom).

width of the cross-section was  $W_{min} = 80$  pixels ( $\approx 63$  mm). A continuous edge curve was then obtained using linear interpolation, after which all elements  $i$  of edge point vectors  $z_{top}(i)$  and  $z_{bottom}(i)$  had numerical values. Then the edge point vectors were filtered with a median filter, similarly to the procedure with I-KI images (Fig 7, middle). Further, the columns were normalized to a standard length of  $w = 200$  (Fig 7, bottom). Finally, the cross-section  $\text{Li}^-$  distribution was obtained by averaging the resampled sequences of all columns. The length of a single  $\text{Li}^-$  image of the cross-section was 200 mm. In total, ToF-SIMS images of 25 cross-sections were used in order to determine the  $\text{Li}^-$  distribution.

## Results

The following figures illustrate the starch penetration curves obtained as examples of utilizing the method developed (Fig 8). These curves show differences in starch penetration depending on the surface sizing solids content as starch concentrated on the surface or penetrated more through the sheet based on starch solids content. In addition, a base paper sample with no surface sizing was analyzed in a similar manner as the surface sized samples. Here, some I-KI dyeing of the base paper

sample through a reaction with fibers, fillers and wet end starch can be seen in the starch “penetration” curve of the non-surface sized base paper. Using the Simulated Starch Content distribution calculation, SSC, starch penetration curves were rearranged by normalizing the integrals of the starch penetration curves according to the starch amount measured from the specimens (Eq [4]). The normalized curves (Fig 9) show a logical arrangement of the starch penetration curves according to starch solids content. The starch amount in paper samples is seldom equal at the top and bottom side of paper. Therefore, a direct comparison of the starch distribution curves at each side or as a function of the entire thickness can be complicated. Here, averaging the curves obtained from the top and bottom sides of the paper can be useful. Fig 10 presents examples of such half curves. The top and bottom averaging is obtained from the Simulated Starch Content curves seen in Fig 9.

Fig 11 illustrates the calculated penetration number  $Q_{tot}$  as a function of the starch solution solids used (i.e. 8%, 12%, 15% and 18%). One can observe in Fig 11 that the penetration number described here gives a fairly good picture of starch penetration with different solids contents. Similarly, the Scott bond internal strength measurements are compared against the penetration number. When observing Fig 12 one can suggest that the penetration number  $Q_{tot}$  introduced here can well be used in evaluating the internal strength of the sheet in terms of starch penetration.

Fig 13 presents the lithium ion distribution of a paper sample with a starch solids content of 18% and total starch amount of  $1.8 \text{ g/m}^2$ . Fig 13 shows that the lithium ions were more evenly distributed across the  $z$ -direction of the paper compared to the starch penetration information from the analysis of binary images of the I-KI dyed cross-sections (Fig 8 and Fig 9). In other words, the lithium ion content of the paper in the middle of the sheet is greater than what was expected based on the I-KI distributions. Fig 13 also suggests, that the maximum  $\text{Li}^-$  concentration is not quite on the surface of the cross-section but at a depth of about 5 mm from the surface of the specimen. This observation agrees well with the findings on the I-KI starch penetration curves, where the

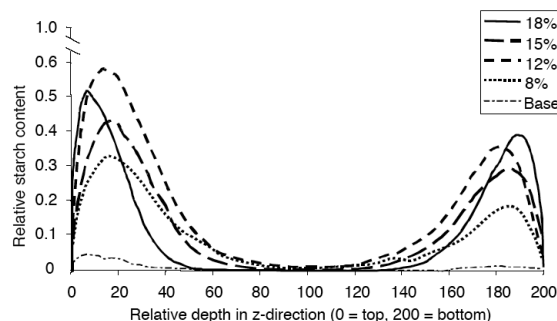


Fig 8. Starch penetration curves with starch amounts of  $1.8 \text{ g/m}^2$ ,  $2.0 \text{ g/m}^2$ ,  $2.0 \text{ g/m}^2$  and  $1.8 \text{ g/m}^2$  with starch solids contents of 18%, 15%, 12% and 8%, respectively. In addition, a reference curve obtained from the base paper sample is presented. The relative starch content (between 0 and 1) in the y-axis describes the occurrence of pixels categorized to contain starch in the  $z$ -directional depth of the sheet.

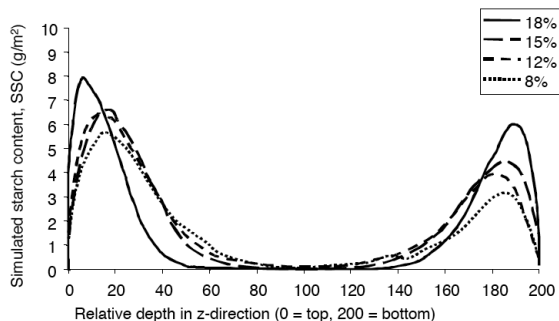


Fig 9. Starch penetration curves normalized to cover an area relative to corresponding starch amounts at each paper sample (i.e. Simulated Starch Content distributions, SSC) at starch amounts of 1.8 g/m<sup>2</sup>, 2.0 g/m<sup>2</sup>, 2.0 g/m<sup>2</sup> and 1.8 g/m<sup>2</sup> with starch solids contents of 18%, 15%, 12% and 8%, respectively.

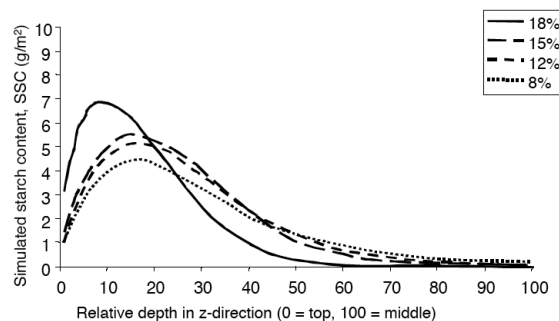


Fig 10. Top and bottom side averaged starch penetration curves with starch amounts of 1.8 g/m<sup>2</sup>, 2.0 g/m<sup>2</sup>, 2.0 g/m<sup>2</sup> and 1.8 g/m<sup>2</sup> with starch solids contents of 18%, 15%, 12% and 8%, respectively. Penetration curves were normalized to cover an area relative to corresponding starch amounts at each point (i.e. Simulated Starch Content distributions, SSC).

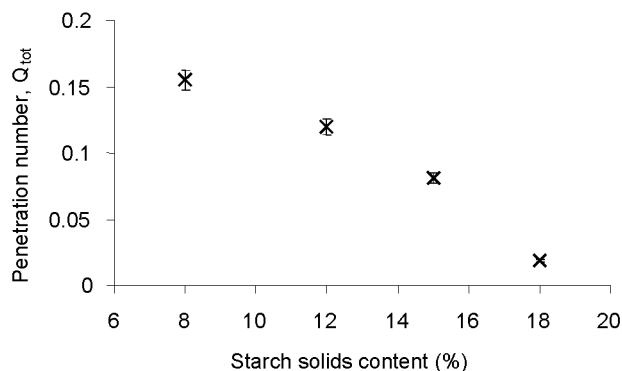


Fig 11. Determined penetration number  $Q_{tot}$  as a function of the starch solids content used (i.e. 8%, 12%, 15% and 18%). The total starch amount was 1.8–2 g/m<sup>2</sup>.

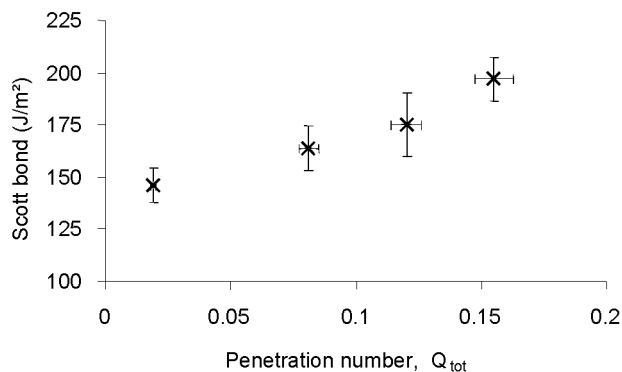


Fig 12. Measured internal strength (Scott bond) as a function of the penetration number. The total starch amount was 1.8–2 g/m<sup>2</sup>.

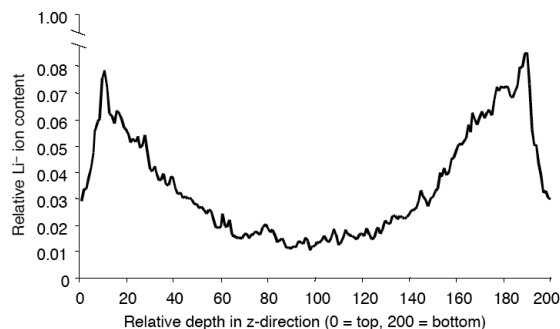


Fig 13. Averaged  $Li^-$  distribution determined for a series of cross-section images (25 images). The starch solids content at the specimen was 18%, and the total starch content 1.8 g/m<sup>2</sup>. The relative  $Li^-$  ion content (between 0 and 1) in the y-axis describes the occurrence of pixels categorized to contain  $Li^-$  ions in the z-directional depth of the sheet.

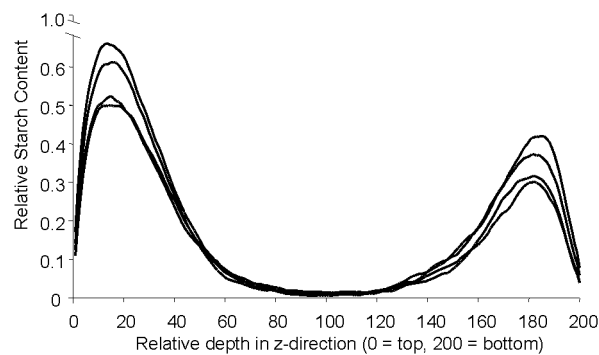


Fig 14. Examples of relative starch content distributions from four parallel specimens, each consisting of averaged information from 16 cross sections. Starch content in the specimen was 2.0 g/m<sup>2</sup> at starch solids content of 12%.

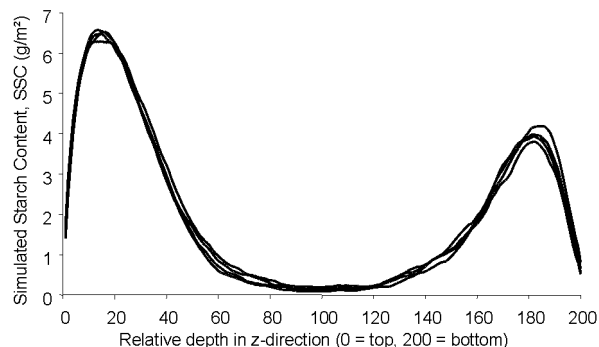


Fig 15. Examples of Simulated Starch Content (SSC) distributions from four parallel specimens, each consisting of averaged information from 16 cross sections. Starch content in the specimen was 2.0 g/m<sup>2</sup> at starch solids content of 12%.

maximum starch penetration was also found to be at a similar depth from the sheet surface.

The accuracy of the method developed can be evaluated by observing starch penetration results from parallel specimens. Four specimens were analyzed in the following figures in order to find out the level of confidence, and further, the repeatability of results with the method developed.

In Fig 14, four parallel relative starch content distributions are compared. One can observe roughly

30% variation in starch content maximum values between the curves. Comparing results based on relative starch content curves alone can therefore be complicated.

However, if the results with the Simulated Starch Content (SSC) distribution are observed, good repeatability of the results can be seen (*Fig 15*). Looking at the Simulated Starch Content distribution and normalizing the curves based on the measured (or targeted) starch amount using *Eq. 6* is therefore the most useful form of plotting the penetration curves. Further, the penetration numbers  $Q_{tot}$  for the specimens compared here give values 0.114, 0.124, 0.104 and 0.131 with an average of 0.118 and standard deviation of 0.012. The method developed for determining the penetration number gives quantitative starch penetration information with coefficient of variation (CV) of 10%.

## Discussion

A quantitative method to evaluate starch penetration was presented in this study. The dyeing of the specimen in the iodine potassium iodine (i.e. I-KI) solution and image analysis of the resulting dyed cross-sections was fast to conduct. The dyeing of the specimen, image acquisition of the dyed cross-sectional surface, and image analysis of the cross-sectional image were defined and specified so as to obtain reproducible and comparable information of quantitative starch penetration. Person-dependent factors affecting the procedure and the results obtained were then minimized. The penetration curves acquired here give an additional tool for studying the effect of papermaking process parameters on the quantitative z-directional penetration of surface sizing starch. The method introduced for obtaining Simulated Starch Content (SSC) distribution curves also gives a helpful tool for characterizing the effect of various process parameters on the starch z-distribution of a sheet. An additional feature of the method is the definition of a dimensionless penetration number  $Q_{tot}$  that can be quantitatively used in comparing the penetration of starch in different paper samples (e.g. produced under different process conditions) to determine the function of any papermaking variable whose contribution to surface sizing starch penetration behavior is of interest. Such variables may be starch viscosities and/or solids contents, linear loads of the MSP unit, roll diameters and hardnesses, as well as such base paper properties as porosity. This information can then be used in optimizing the papermaking process with respect to the penetration of starch. The results presented here showed a good correlation between the starch solids content and the internal strength of the sheet, for example. The method described will open new possibilities for describing starch penetration compared to the conventionally used qualitative evaluation of iodine stained cross-sections.

One must note that the penetration curves described here should, in principal, not be directly interpreted as

starch amount distributions due to the method used in determining the curves. Here, the method is based on evaluating whether the individual pixels across the cross-section contain starch or not – instead of quantitative information of the starch content at that particular location. Nevertheless, the simulated starch content (SSC) distribution curves presented seem to also represent the expected relative starch amount distribution in the z-direction quite well.

The starch penetration curves were also compared against  $\text{Li}^-$  distributions obtained through ToF-SIMS, representing the distribution of the starch solution in the z-direction, using  $\text{LiCl}_2$  as a marker for starch. The comparative ToF-SIMS results repeat the observation made with I-KI dyed and image analyzed cross-sections showing a drop of starch content in the 5  $\mu\text{m}$  layer of the topmost surface of the sheet. However, the  $\text{Li}^-$  distributions show a deeper penetration compared to the I-KI curves. This may be explained through the  $\text{LiCl}_2$  marker migrating through the fiber network with the water in the starch solution.

In conclusion, the quantitative starch penetration analysis method presented here describes very well changes in starch penetration against penetration-related process parameters and paper properties, such as starch solids content or viscosity, or the internal strength of the sheet. This method will provide a new tool for papermakers for optimizing and fine tuning starch penetration-related process parameters and the properties of paper in paper or board surface sizing.

---

## Acknowledgements

The authors wish to thank Mr. Antti Vuorivirta of Raisio Chemicals for his years-long work in developing the cross-sectional imaging procedures utilized as a basis for the development of this starch penetration analysis method. Mr. Timo Laine of Raisio Chemicals provided a lot of essential information and helped to evaluate the results. We would also like to warmly thank Ms. Merja Taiminen of VTT Processes for her valuable contribution to the further development of the sample preparation and imaging of the cross-sections.

---

## Literature

- Ahluross, J. and Grön, J.** (1998): Influence of Base Paper Filler Content and Pre-calendering on Metered Film Press Coating – Part I: A Coating Process Study. Proc, TAPPI Coating / Papermakers Conference, TAPPI Press, Atlanta, GA, USA, pp. 899.
- Allem, R.** (1998): Characterization of Paper Coatings by Scanning Electron Microscopy and Image Analysis, *J. Pulp and Paper Sci.*, 24(10), pp. 329.
- Allem, R., Uesaka, T.** (1999): Characterization of Paper Microstructure: A New Tool for Assessing the Effects of Base Sheet Structure on Paper Properties, Proc. Microscopy as a tool in Pulp and Paper Research and Development Symposium, Stockholm, pp. 21 and 52.
- Bailey, D.F., Bown, R.** (1990): The Use of Pigments At The Size Press – A European view, TAPPI Papermakers Conference, Proc, TAPPI Press, Atlanta, GA, USA, pp.199.
- Bailey, J. H. E. and Reeve, D. W.** (1994): Spatial distribution of trace elements in black spruce by imaging microprobe secondary ion mass spectrometry. *J. Pulp and Paper Sci.*, (20) J83-J86.
- Barratte, C., Dalphond, J.E., Manglin, P.J. and Valade, J.L.** (1997): An automatic determination of threshold for the image analysis of prints, *Advances in Printing*

Science and Technology, Proc. IARIGAI 23rd research conference, pp. 451.

**Bergh, N.-O.** (1984): Surface Treatment on Paper with Starch from the Viewpoint of Production Increase, XXI EUCEPA International Conference, Volumen 2, Conferencias nos 23 a 43, Torremolinos, Spain, pp. 547.

**Bergh, N.-O., Åkesson, R.** (1988): Upgrading of Supercalendered Papers for Offset Printing, Proc. TAPPI Coating Conference, TAPPI Press, Atlanta, GA, USA, pp. 73.

**Brinen, J. S. and Kulick, R. J.** (1995): SIMS imaging of paper surfaces. Part 4. The detection of desizing agents on hard-to-size paper surfaces. International Journal of Mass Spectrometry and Ion processes 143 pp. 177.

**Chinga, G. and Helle, T.** (2002): Structure characterisation of pigment coating layer on paper by scanning electron microscopy and image analysis, Nordic Pulp Paper Res. J., 17(3), 307.

**Dickson, A.** (2000): Quantitative analysis of paper cross sections, Appita J., 53(4), pp. 292.

**Fineman, I., and Hoc, M.** (1978): Surface Properties, especially linting, of surface sized fine papers, Tappi J., 61(5), pp. 43.

**Hansson, J. A., Klass, C. P.** (1984) High Speed Surface Sizing, Tappi J., 67(1), 64.

**Hoyland, R., Howarth, P., Whitaker, C. and Pycraft, C.** (1977): Mechanisms of the size press treatment of paper. Paper Technology and Industry, 18(8), pp. 246

**Kimpimäki, T., and Rennes, S.** (2000): New Surface Sizing Concept Significantly Reduces Porosity, Liquid Penetration and Surface Roughness, Paperi Puu – Paper and Timber 82(2), pp. 525.

**Kulick, J. and Brinen, J. S.** (1998): Probing paper surfaces with ToF SIMS: A new problem solving tool, Tappi J., 81(2), pp. 152.

**Lipponen, J., Grön, J., Bruun, S-E and Laine, T.** (2002): Surface Sizing with Starch Solutions at High Solids Contents. Proc. TAPPI Metered Size Press Forum, TAPPI Press, Atlanta, GA, USA, pp. 129.

**Mendham, J., Denney, R., Barnes, J., Thomas, M.** (2000): Vogel's Textbook of Quantitative Chemical Analysis, Prentice Hall, New York, NY, USA, pp. 806.

**Peterson, A and Williams, L. C.** (1992): Determining Paper-Coating Thickness with Electron Microscopy and Image Analysis, Tappi J., 74(10), pp. 122.

**Preston, J.S., Elton, N.J., Husband, J.C., Legrix, A., Heard, P. J. and Allen, G.**

**C.** (2000): SIMS analysis of printed paper surfaces to determine distribution of ink components after printing, Tappi International Printing & Graphic Arts Conference, TAPPI Press, GA, USA, pp. 101.

**Rantanen, R., Westergård, S.** (1987): Valmet's latest development in surface treatment, Proc. The World Pulp and Paper Week: New Available Techniques and Current Trends, SPCI – The Swedish Association of Pulp and Paper Engineers, Sweden, pp. 698.

**Ryder, D.J.** (1997): Practical Experiences with a SymSizer, Proc. PITA Coating Conference, PITA Coating Working Group, pp. 49.

**Sollinger, H.-P.** (1988): Speedsizer, Proc. TAPPI Coating Conference, TAPPI Press, Atlanta, GA, USA, pp. 145.

**Tehomaa, J., Palokangas, E., Mäkimattila, J., Tuomisto, M.** (1992): High Speed Surface Sizing of Fine Papers: A Comparison of Different Techniques, Proc. TAPPI Papermakers Conference, TAPPI Press, Atlanta, GA, USA, pp. 353.

**Tovey, N.K. and Hounslow, M.W.** (1995): Quantitative micro-porosity and orientation analysis in soils and sediments, J. Geological Society 152, pp. 119.

**Wight, E.W.** (1988): Operation and Application of the Blade Metering Size Press, Proc. Tappi Coating Conference, TAPPI Press, Atlanta, GA, USA, pp. 123.

**Williams, G. J. and Drummond, J.G.** (1994): Preparation of large Sections for the Microscopical Study of Paper Structure, Proc. Tappi Papermakers Conference, TAPPI Press, GA, USA, pp. 517.

**Zimmerman, P. A. and Hercules, D. M.** (1995): Direct quantitation of alkylketene dimers using Time-of-Flight secondary ion mass spectrometry. Anal. Chem. (67), pp. 2901.

**Zsoldos B. and Sebess I.** (1975): Die Bestimmung des Stärkegehaltes von mit modifiziert Stärke behandelten Papieren. Zellstoff und Papieren (10) pp. 299–302.

*Manuscript received November 21, 2003*

*Accepted April, 2004*